$(e,2e)$ ionization studies of alkaline-earth-metal and alkali-earth-metal targets: Na, Mg, K, and Ca, from near threshold to beyond intermediate energies

Andrew James Murray*
School of Physics and Astronomy, University of Manchester, Manchester M13 9PL, United Kingdom
(Received 2 September 2005; published 21 December 2005)

A comprehensive set of experimental data is presented for the electron impact ionization differential cross sections of sodium, magnesium, potassium, and calcium. A coplanar symmetric geometry was chosen for these $(e,2e)$ coincidence studies, the energies ranging from near threshold to around fifteen times the first ionization potential. The results reveal a complex structure in both angle and energy which depends on the chosen target. Similarities and differences in the overall structure are found for the targets which have been studied. The results are compared to the measured cross section for helium over the same incident energy regime. The calcium results are also compared to recent theoretical calculations using a distorted wave Born approximation and the convergent close coupling method. Clear discrepancies are found between both theories and with experiment.

DOI: 10.1103/PhysRevA.72.062711 PACS number(s): 34.80.Dp

I. INTRODUCTION

Determination of the electron-impact ionization cross sections for atomic targets is one of the most fundamental problems in collision physics. This process is studied in detail by determining the complete kinematics of the interaction in a so-called $(e,2e)$ experiment, where the incident, scattered and ejected electron momenta are ascertained. In these experiments all knowledge about the reaction is determined, apart from the spin. The reaction can be written as

$$e_0(\mathbf{k_0},E_0)+A\rightarrow e_a(\mathbf{k_a},E_a)+e_b(\mathbf{k_b},E_b)+A^+, \qquad (1)$$

where $\mathbf{k_0},\mathbf{k_a},\mathbf{k_b}$ represent the momenta of the incident, scattered, and ejected electrons of energy E_0,E_a,E_b, respectively. A and A^+ represent the target and resulting ion in their ground states. From energy conservation an additional equation can be written:

$$E_0=E_a+E_b+V_{\text{ion}}, \qquad (2)$$

where V_{ion} is the potential required to ionize the target.

From these equations it is clear that a very wide range of reactions and geometries may be selected, and so it is necessary to restrict experiments to measure a *subset* of the total possible events. High energy experiments (>100 eV) have been carried out for a number of years by several research groups, providing a rich and diverse set of data from different targets [see, e.g., [1–9] and references therein]. Theoretical groups have also made great advances in solving the dynamics of the reaction at these energies, by adopting models such as the Born approximation and by using distorted waves to represent the incident and outgoing electrons [10–14]. The agreement found between experiment and theory means that the high impact energy problem can be considered as mostly resolved.

By contrast, the energy regime between threshold and ~100 eV does not show such good agreement between experiment and theory. For incident electron energies ranging from $R=3$ to 7 times the ionization potential, the probability for ionization is a maximum *for all targets* [15]. This intermediate energy regime is therefore of great significance from a practical point of view, since most ionization events occur here.

Unfortunately, this energy regime is also one of the most difficult in which to work. Significant experimental challenges arise due to the requirement to accurately control the incident electron beam momentum, while simultaneously determining the momenta of the outgoing electrons. Theoretically, reactions in this regime are extremely challenging to model since many approximations used at higher energies fail. In the intermediate energy regime the dynamics of the reaction are controlled by factors which must all be considered on an equal footing. These factors include long-range distortions in the wavefronts describing incident, scattered and ejected electrons; multiple collisions between the incident electron, target electrons and ionic core; polarization of the target atom and ion as the reaction progresses; exchange effects, including those where the incident electron exchanges with the core electrons; and postcollisional interactions (PCI) which occur over large distances as the electrons emerge from the reaction zone. This energy regime therefore provides the most demanding tests of all current, and any future collision theories.

The computer controlled and computer optimized $(e,2e)$ spectrometer at Manchester used in the experiments presented here was designed to operate at incident electron energies from ~10 eV to 300 eV, and so encompasses the intermediate energy regime for all atomic targets [16]. The spectrometer was commissioned in 1991, and has been operating continuously since that time, collecting information on targets which are in the gas phase at normal temperatures [17–20]. The spectrometer has the additional advantage that it can operate from a coplanar geometry (where the incident, scattered and ejected electrons occupy a single plane) through to the perpendicular geometry (where the scattered

*Email address: Andrew.Murray@Manchester.ac.uk

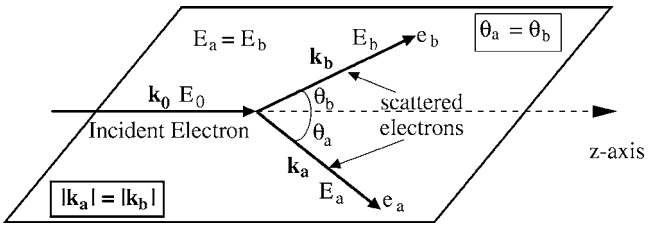

FIG. 1. The coplanar symmetric $(e,2e)$ geometry adopted in these experiments. The incident electron energy ranged from 10.1 eV to 67.7 eV, depending upon the target under study. The outgoing electron energies were selected to be equal, and ranged from 2 eV to 30 eV.

and ejected electrons emerge perpendicular to the incident beam direction). As such, ionization measurements can be conducted over the full three dimensions, and this has lead to the discovery of new quantum interference effects which have yet to be fully explained [21].

In the experiments detailed here, a coplanar geometry was chosen, where the polar angles of the electrons (θ_a, θ_b) with respect to the incident electron beam direction were set equal, $\theta_a = \theta_b = \theta$. An additional constraint was that the energy of the selected outgoing electrons was also equal, $(E_a = E_b)$, as shown in Fig. 1. This *coplanar symmetric* geometry provides the most demanding test of theory, as the electrons must be treated equally. Further, since the interaction time between the outgoing electrons occurs over a long range due to their equal energies, the effects of postcollisional interactions on the measured signal is maximized.

The motivation for carrying out these difficult new experiments using alkali-metal and alkali-earth-metal vapors was to look for similarities and differences between the cross sections when ionizing these targets, and to compare the new results to noble gas-phase targets such as helium. Previous measurements [22] ionizing calcium (with two electrons in the 4*s* valence shell) show marked differences between theory and experiment [23,24]. It was therefore decided to significantly enhance the body of experimental data, by measuring the ionization cross section for magnesium (two electrons in the $3s^2$ valence shell), potassium (one electron in the 4*s* valence shell) and sodium (one electron in the 3*s* shell). In this way the effects of correlation between valence electrons can be considered, the effects of different closed and open shells of inner electrons can be studied, and the differences between theory and experiment found for calcium can be explored.

The data presented here was collected over a period of three years using the $(e,2e)$ spectrometer in Manchester. Collection of data at energies near threshold provided significant experimental challenges, due to deposition of metal vapors onto different critical elements in the spectrometer, and subsequent charging of these surfaces once the electron beam was operating. Each target produced different problems, ensuring that data collection was always interesting. At higher incident energies the effects of deposition played a lesser role, however these challenges were compounded by very low coincidence count rates in the backward scattering direction. These low coincidence yields produced large uncertainty and subsequent variations in the data, which can be seen in the results presented here.

This paper is divided into eight sections. Following this introduction the experimental apparatus is discussed in Secs. II and III, in particular where changes were made to the existing spectrometer to allow metal vapor targets to be studied. The conditions used in the experiments are detailed, as well as the different experimental challenges which were faced. The energy calibration used throughout data collection is described in Sec. IV.

The new experimental results are presented in Secs. V–VII. Low energy results up to ~10 eV above threshold are presented in Sec. VI, and are compared to low energy data from helium. In this energy regime PCI and exchange will play a significant role, and so the Wannier model [25] is considered together with results from a new DWBA model [23] and a CCC model [24] for calcium. Section VII presents the complete set of data up to 60 eV above threshold, and compares these data again with helium and theory. The differences found between theory and experiment for calcium (as noted above) are then considered in terms of the results from the new targets. Section VIII draws conclusions from the data, and presents an analysis of possible future directions.

II. THE EXPERIMENTAL APPARATUS

The experimental apparatus used in Manchester is a fully computer controlled and computer optimized $(e,2e)$ spectrometer which is unique in several ways. The spectrometer adopts a technique that allows a standard personal computer to maintain operating conditions at their optimum for many days, prior to intervention [16]. The routine uses a Simplex method [26] to adjust the voltages on lens elements within the electron gun and analyzers so as to optimize a given parameter. As an example, if the parameter for optimization is the output current of the electron gun, the routine will adjust the electrostatic lens focusing and deflectors within the gun so as to maximize this current onto a Faraday cup. Alternatively, if the rate of electrons detected by a channeltron in an analyzer are to be optimized, the lens and deflectors in the analyzer will be adjusted so as to maximize these counts. Under these control systems, the spectrometer operates 24 hours a day, allowing reliable and consistent data to be accumulated over many months. This precise control is necessary when the cross section for ionization is very low, as drifts in the spectrometer tuning conditions over time are corrected.

Another unique feature of the spectrometer is the ability to move from a coplanar geometry to the perpendicular geometry. This is facilitated by moving the electron gun, while rotating the electron energy analyzers in the detection plane. The analyzers are located on two horizontal turntables as shown in Fig. 2, so that their angles can be independently adjusted. The electron gun (shown here in the perpendicular plane) is situated on a yolk rotating around an axis which accurately passes through the center of rotation of the analyzers. The interaction region is located where these two axes meet.

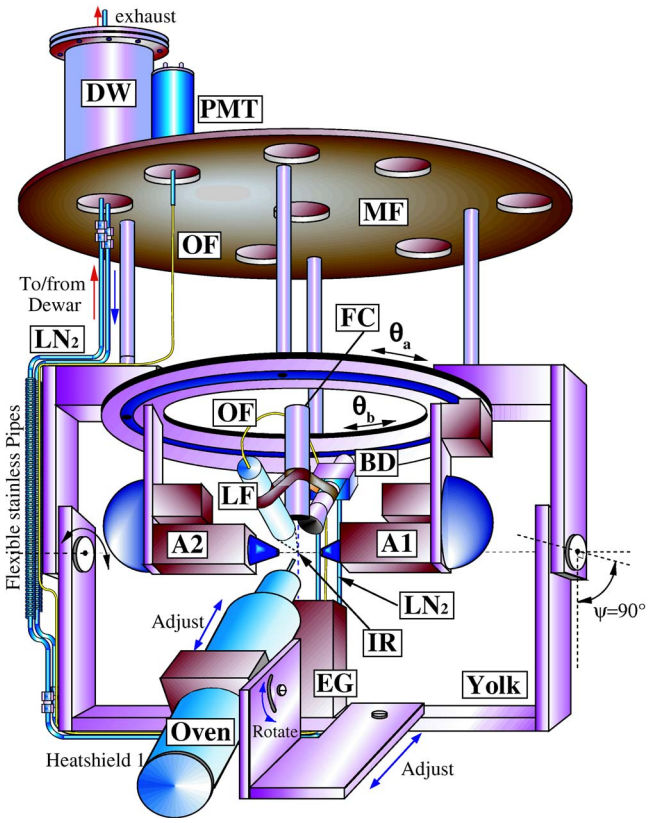

FIG. 2. (Color online) The experimental apparatus, configured in the perpendicular plane to show the position of different components. The analyzers A1 and A2 move on separate turntables to map out the horizontal detection plane through angles θ_a, θ_b. The electron gun (EG), atomic beam oven, Faraday cup (FC), beam dump (BD), and a lens-optical fiber monitoring system (LF) all mount from the yolk so as to move together from $\psi=0°$ (coplanar geometry) to $\psi=90°$ (perpendicular plane). The beam dump was fed from a liquid nitrogen Dewar (DW) via flexible stainless steel pipes. An optical fiber (OF) directed light from the interaction region to an external photomultiplier tube (PMT) mounted on the main vacuum flange (MF).

Also attached to the yolk assembly is a Faraday cup situated 30 mm beyond the interaction region on the opposite side to the gun, an oven which houses the target atoms, a beam dump located 40 mm from the interaction region opposite the oven exit, and a lens-fiber optical assembly used to monitor fluorescence from the interaction region. Each component can be independently and accurately adjusted. All components rotate with the electron gun on the yolk assembly, so that the overlap between the electron beam and atomic beam remains constant for different selected geometries.

The analyzers consist of hemispherical energy selectors coupled to three element input lenses which image electrons from the interaction region onto the (virtual) entrance aperture in the selector. Electrons which are energy selected inside the hemispheres exit through a second (real) 1 mm aperture before being detected by a Photonis X719BL channel electron multiplier [27]. The analyzers can rotate without restriction from $\theta=35°$ through to $\theta=125°$ when operating in a coplanar symmetric geometry.

The atomic beam emanating from the oven which passes through the interaction region is collected by a 310-grade stainless steel beam dump. The beam dump is maintained at an operating temperature of −180 °C by feeding liquid nitrogen from a dewar [28] located on the top flange through a chamber enclosing the beam dump. The 5 liter capacity dewar maintains liquid nitrogen in this chamber using a gravity feed through flexible stainless steel pipes, gases due to vaporization of the liquid being exhausted through the return pipe. The dewar level is monitored by a pair of green LED's immersed inside the dewar at different levels, electronic control systems maintaining the level between the LED's [29]. With the oven at normal operating temperature, the rate of loss of liquid nitrogen is less than 1.2 liters per hour.

Fluorescence from excitation of the atomic beam by the electron beam is normally collected by a 12 mm diameter aspheric lens which images the interaction region onto a 400-μm-core multimode fiber. The optical fiber passes through a custom-built vacuum feedthrough so that fluorescence exiting the fiber is directed through an interference filter onto the bialkali photocathode of a single photon counting photomultiplier tube. Fluorescence is usually monitored in this spectrometer to optimize the electron gun, as it allows the electron beam to be focused onto the interaction region accurately defined by the optical lens assembly [16]. Unfortunately, all metal vapor targets used in the present studies rapidly contaminated the optical system by depositing onto the lens, rendering it opaque within five days. Optimization of the electron gun was therefore restricted to maximising the current in the Faraday cup for all data collected here.

The atomic beam oven used in these experiments was a modified version of that used for calcium [30]. Figure 3 shows the design adopted. The oven consists of a chamber constructed from a single 12.7 mm bar of 310 grade stainless steel, bored out to take a charge of either calcium pellets, magnesium turnings, sodium or potassium in the lower crucible. The output nozzle is constructed from molybdenum with an external diameter of 2 mm and internal diameter of 1.2 mm. Molybdenum is used as it is nonmagnetic, has a very high melting point and is chemically inert to the different atomic beams being produced.

The heaters surrounding the lower and upper crucibles are constructed using twin-core thermocoax [31] wound onto copper heater jackets surrounding the crucible. A third intermediate copper jacket sandwiched between the heaters conducts heat to the junction between lower and upper crucibles. This jacket was found to be essential when using calcium and magnesium, which directly sublime to the gas phase. Without the intermediate jacket in place, vapor was found to recondensed at the junction inside the oven until a blockage occurred. Once blocked, the oven ceased to emit atoms and had to be cleaned. The intermediate copper jacket solved this problem by ensuring the junction remained hot. A copper cylinder is also fitted around the molybdenum nozzle to conduct heat from the upper heater to the nozzle, preventing blockages within the nozzle.

The oven and heater assemblies are surrounded by four heat shields, as shown in the figure. These reflect heat back into the oven assembly, reducing the power needed to heat

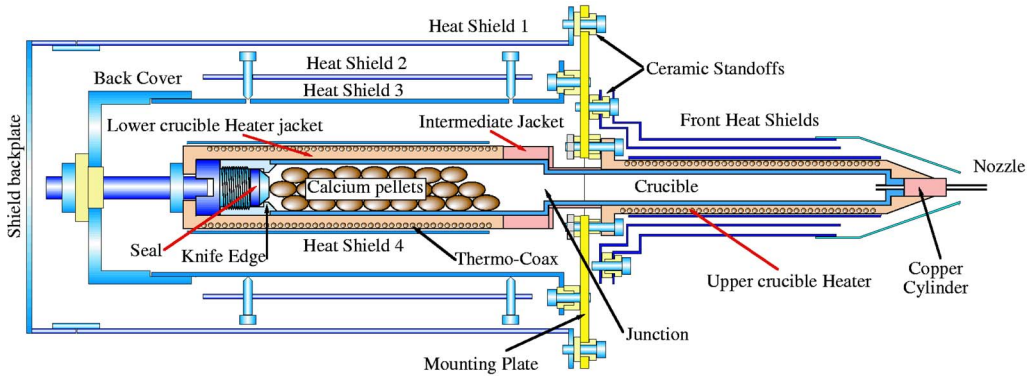

FIG. 3. (Color online) The atomic beam oven used in this study. The oven is comprised of a lower and upper crucible which were separately heated. The seal on the oven was constructed of 310 grade stainless steel for Ca and Mg, and was of oxygen free copper for Na and K. The hypodermic nozzle was of molybdenum. For details, see text.

the oven to the desired temperature. The heat shields are thermally insulated from the oven mount using ceramic standoffs. The oven crucible can be removed from the heater and shield assembly by releasing the back cover from heat shields 1 and 2, then drawing out the crucible. This allows the charge in the oven to be refilled without losing alignment to the interaction region.

An important difference between the oven in [30] and the new oven presented here is the seal used to close the crucible following filling. In the new design, this seal is a tapered plug which locates into the back of the crucible, and which is secured against the inner crucible knife edge using a screw fitting. For experiments using calcium and magnesium, the plug is constructed from 310 grade stainless steel. This was found to be necessary particularly for hot calcium, which reacts vigorously with a seal made of copper.

By contrast, for crucible charges of potassium and sodium the plug is constructed of oxygen free copper, since this is efficiently cut by the internal knife edge to produce a secure metal to metal seal. Copper is found to react only slowly with these alkali metals when they are liquid, so can be used effectively for long periods. In early work with potassium, the stainless steel plug was used with dangerous consequences, since liquid potassium passed the seal, flowed around the screw fitting and leaked between the lower heater and oven body. Upon opening the spectrometer a large and potentially explosive quantity of metal had to be removed between the oven and heater, and the oven was damaged beyond repair. Using a copper seal eliminated this problem.

Filling of the oven crucible was always carried out in an argon atmosphere inside a glove bag for safety reasons, and to ensure that the charge did not oxidize. Magnesium reacts slowly with air, and so required only minor safety procedures when filling. Calcium reacts more vigorously, whereas sodium reacts strongly with any water vapor in air. Potassium in particular can be dangerous, so caution was required when filling the oven. Prior to removal of the filled oven from the glove bag, the seal and screw assembly were secured, and a close-fitting plug was inserted into the molybdenum nozzle. The nozzle plug was only removed immediately prior to the spectrometer being evacuated, ensuring that the atmosphere inside the oven body remained predominantly argon until under vacuum.

The heaters in the oven were operated using two variable constant current supplies that could operate up to 65VDC. The heater jacket temperatures were monitored by type-K thermocouples again supplied by thermocoax [32]. The oven was heated slowly for four hours until it reached operating temperature, which depended on the type of charge. By using constant current supplies, it was not necessary to provide feedback control to ensure the oven stabilized at a constant temperature. The oven could be maintained at the working temperature with an accuracy of ±0.5 °C for several weeks.

The operating temperatures found to produce satisfactory $(e,2e)$ coincidence signals for each target are given in Table I.

III. EXPERIMENTAL CHALLENGES WITH DIFFERENT TARGETS

A number of difficulties were found when operating with different targets. The alkali-metal targets both pass through a liquid phase prior to the gas phase, whereas the alkali-earth-metal targets directly sublime from the solid phase to the gas phase during operation. The problems with different targets within the oven crucible have already been discussed above.

A further problem when operating the oven at high temperatures was found due to indirect heating of surrounding components in the spectrometer. In particular, expansion of the gear assembly that operated the analyzer turntables caused binding between the gears, preventing movement. This was alleviated by reducing the tightness of the gear meshing when cold. The temperature of the surroundings was continuously monitored using four copper-constantan

TABLE I. Operating temperatures of the oven for different targets.

Target atom	Lower heater temp.	Upper heater temp.
Sodium	330 °C	350 °C
Magnesium (sublimes)	545 °C	575 °C
Potassium	245 °C	255 °C
Calcium (sublimes)	600 °C	630 °C

thermocouples, as this allowed local heating problems to be addressed.

The main problem with these metal vapor targets was due to deposition of vapors onto sensitive components in the spectrometer. The apparatus at Manchester adopts an open interaction region, which is essential to allow full movement in three dimensions. Hence any insulating surface contaminants could charge up, due to stray electrons from the gun. These surfaces then vary the field in the interaction region, resulting in changes in the apparent energy of the $(e,2e)$ process.

Although a liquid nitrogen cooled beam dump was used throughout these experiments to help confine the atomic beam, it was impossible to prevent deposition from occurring elsewhere. It was therefore necessary to perform regular energy calibration runs throughout data collection, as discussed in the next section. Each target was found to produce different problems, partly due to chemical reactions between hot atoms and the contaminated surfaces. The shields around the analyzers in the spectrometer are constructed of advance (constantan) sheet, and these were found to react with hot calcium, potassium, and sodium. All surfaces near the interaction region were constructed of molybdenum, which was inert to reactions, and could be easily cleaned. Deposition still occurred on these surfaces while the oven was running, which again contributed to small variations in the overall energy.

The beam dump was constructed from stainless steel, since this was also found inert to the hot atoms, and could be easily cleaned. Calcium produced a black deposition on the beam dump and other cold surfaces. This black deposit did not appear to be pure calcium (which has a dull silver color), however it remains unclear how it is produced in vacuum. The deposit could be removed in water, leaving a clean metal surface. Since calcium produced the largest changes in potential of all targets studied, it is thought that this deposition was nonconducting, leading to significant patch fields.

Magnesium proved to have little effect on the energy of the interaction, due to a very clean deposition onto the beam dump. Since magnesium is not particularly reactive in air, deposition onto surfaces inside the spectrometer remained relatively conductive when the system was opened. The main problem was found when cleaning contaminated surfaces of magnesium, as a weak solution of sulphuric acid was required to remove the deposition. This acid also reacted with the advance shields, and so care was required when using this. In general, magnesium proved to be the easiest of all targets to use.

Sodium and potassium produced different problems to calcium and magnesium, due to the reactive nature of these atoms when exposed to air. When opened for maintenance, surface layers of both alkali metals immediately started to foam and react with water vapor in the air. This produced potassium and sodium hydroxide, which also reacted with the advance shields. Upon opening the system it was therefore necessary to quickly remove all shielding from the spectrometer and deposit these in a water bath, thereby removing both the alkali metal and its hydroxide. The shields were then thoroughly cleaned and inspected for damage prior to refitting. It was far more difficult to clean components of the spectrometer which could not be easily removed, without complete dismantling of the spectrometer. Fortunately these components were sufficiently distant from the interaction region that patch fields due to surface charging were not found to be significant.

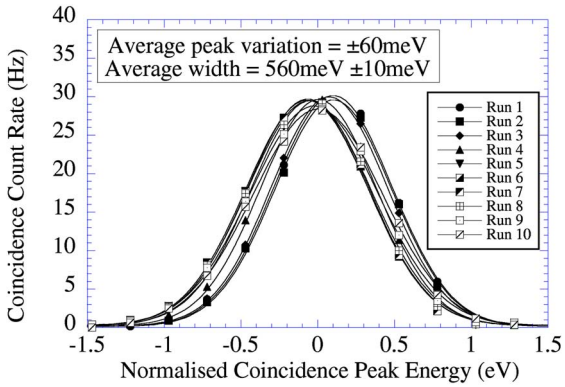

FIG. 4. (Color online) Normalized coincidence energy calibration data fitted to a Gaussian to establish the relative width of the coincidence energy peak, and stability over time. The results are for a calcium target, where the oven had been operating for four days prior to this data being collected. Ten calibration runs taken over a 15 hour period are shown. The variation in peak position over this time was $\sim\pm 60$ meV, the peak half width being 560 ± 10 meV.

IV. ENERGY CALIBRATION

As noted above, it was necessary to establish the energy of the interaction during different experiments. To facilitate this, coincidence energy calibration measurements were regularly made to establish optimum operating conditions. These were conducted by varying the incident electron energy while monitoring coincidence yield, thereby producing an energy calibration curve which was fitted to a Gaussian, as shown in Fig. 4. This calibration was conducted each time the analyzers finished a sweep around the detection plane.

To ensure that the calibration procedure was reasonable, experiments were conducted from a helium target while the oven was operating, by simultaneously feeding helium from a hypodermic needle into the interaction region. Scattering experiments monitoring the elastic resonance at 19.334 eV [33] were conducted to establish the variation of the incident beam energy with time, as deposition occurred. Experiments monitoring ejected electron spectra from helium were also conducted, since these spectra only depend on the energy of the *outgoing* electrons. From these studies it was established that the dominant variation in energy was due to changes in the incident beam energy. The analyzer residual energies were therefore considered to be stable and accurate, and the energy of the incident beam was varied accordingly. Final checks were carried out by monitoring inelastic spectra from the target using both analyzers simultaneously, to ensure they were both set to the same residual energy.

The variation in energy due to deposition in the spectrometer depended on the chosen target. For magnesium, there was little variation over time. For potassium and sodium, variations around 200–300 meV were typical. Calcium pro-

duced the largest change, with up to 1 eV variation over a period of several days. These energy shifts occurred rapidly upon commencement of the experiment, gradually reducing until a stable operating condition (within around ±50 mV) was found, as shown in Fig. 4. As these changes were experiment and target dependent, a variation of ±500 mV on the incident electron energy is considered a reasonable estimate of the energy uncertainty for the data presented here.

V. EXPERIMENTAL RESULTS

Since a large body of experimental data is being presented, it was decided to discuss this in two different outgoing electron energy regimes, ranging from threshold to 10 eV excess energy following ionization, and from ~10 eV through to 60 eV excess energy. The results are compared to helium over the same energy range, and with theoretical calculations for calcium (no other target has yet been modeled).

Of interest (and conjecture) is how these different regimes might be defined. In the discussions below the excess energy is used, since postcollisional interactions critically depend on this excess energy for the symmetric geometries used here. An alternative is to consider the ratio R between the incident energy and the ionization energy. The ionization potentials for the targets studied here are all relatively low, being 4.34 eV (potassium), 5.14 eV (sodium), 6.11 eV (calcium), and 7.65 eV (magnesium). Hence in these experiments the ratio R varies from a minimum value of $R=1.66$ for calcium through to $R=14.8$ for potassium. By contrast, the ionization potential for helium is 24.6 eV, and so R varies from $R=1.12$ through to $R=3.04$ for the results presented here.

Section VI details the results from near threshold through to 10 eV above threshold, where PCI dominates the ionization process in helium. Experiments on metal vapor targets are very difficult in this energy regime, and so the results for Na, Mg, and K are at 6 eV and 10 eV above threshold. It was possible to reduce this to 4 eV and 6 eV above threshold in calcium. By contrast, results have been taken ionizing helium by Selles and co-workers down to less than 2 eV above threshold [34], and by the Manchester group between 3 eV and 10 eV above threshold [17,35]. These lower energies were possible since the difficulties associated with metal vapors detailed above are absent in helium, and the incident energy ($E_0 \sim 25-35$ eV) is in a range where the electron gun operates reliably.

Section VII details the complete data sets for each target up to 60 eV above threshold, to indicate how the structure evolves over a wide range of energies. Existing results for helium are shown for comparison, as are examples of theoretical results for calcium taken from the DWBA model of [23] and CCC model of [24].

VI. LOW ENERGY DCS RESULTS (INCIDENT ENERGY UP TO 10 eV ABOVE THRESHOLD)

Figure 5 shows the data obtained at $E_a=E_b=3$ eV and 5 eV for Na, Mg, and K, and at $E_a=E_b=2$ eV, 3 eV, and 6.75 eV for Ca. The data are normalized to unity at $\theta=45°$, since absolute measurements were not obtained. The results are presented on a logarithmic scale, the scattering angles being constrained between $\theta=35°$ and $\theta=125°$ by the Faraday cup and electron gun, as noted in Sec. II. The experiments were performed by collecting data at a given angle for a set time, then moving each analyzer by 5°, reoptimizing the analyzer lens voltages and recommencing data collection. After one complete sweep of the detection plane the spectrometer was completely reoptimized, an energy calibration was performed, and data collection recommenced. Up to fifteen sweeps of the detection plane were performed at each energy, the data presented here being an average over all measurements. The uncertainties shown in the data were taken from this averaging, and an uncertainty of $\pm 3°$ in the scattering angle was taken from the entrance apertures to the analyzers.

The data is presented on a scale which spans five orders of magnitude, to allow comparison with the results for helium in Fig. 6. Several features are immediately striking from the data. The overall structure of the cross sections for Mg, K, and Ca are similar, whereas Na displays a very different angular variation to the other targets. The forward peak in Na is broad, and little backwards structure appears, apart from a slowly varying region beyond $\theta \sim 100°$ where the cross section remains relatively constant. By contrast, the results for the other targets show forward and backward scattering peaks, with potassium and calcium displaying a third peak around 80° and a minimum around 100°. This middle peak is most clearly visible in calcium at $E_a=E_b=2$ eV. A middle structure is predicted by both the DWBA model [23] and CCC model [24], although neither reproduce the correct relative magnitude. The magnesium cross section at $E_a=E_b=3$ eV does not show a middle peak, and has a minimum at $\theta \sim 80°$.

At the slightly higher energy of 5 eV, the cross section for Mg continues to display a two peak structure. The minimum between the peaks is more pronounced and is at $\theta \sim 90°$. At this energy the minimum in potassium is significantly deeper, the middle peak is still visible as a small "shelf" structure and the relative cross section between forward and backward peaks is larger. The data for calcium at the slightly higher energy $E_a=E_b=6.75$ eV is similar to potassium, however both the minimum and middle "shelf" structure are less pronounced (it should be noted that the results for Ca were taken prior to measurements from other targets, and so are at slightly different energies).

Low energy ionization cross sections for helium are shown in Fig. 6, to allow comparison with the alkali-metal and alkali-earth-metal targets. The results are again normalized at $\theta=45°$, and are presented for energies $E_a=E_b=1$ eV [34], 1.5 eV, 2.5 eV, and 5 eV [17,35]. The results at 2.5 eV and 5 eV are nearest in energy to those in Fig. 5. The data at 1 eV and 1.5 eV are reproduced here to indicate the very significant effects of postcollisional interactions when ionizing helium. At these energies the Wannier model [25] reproduces the data well. This model assumes the interaction is dominated by PCI, the long range Coulomb interaction between outgoing electrons of equal energy forcing them to emerge opposite each other at $\theta_a=\theta_b=90°$. In this case, forward and backward scattering processes occurring during the reaction evolve into the single peak structure, due to the

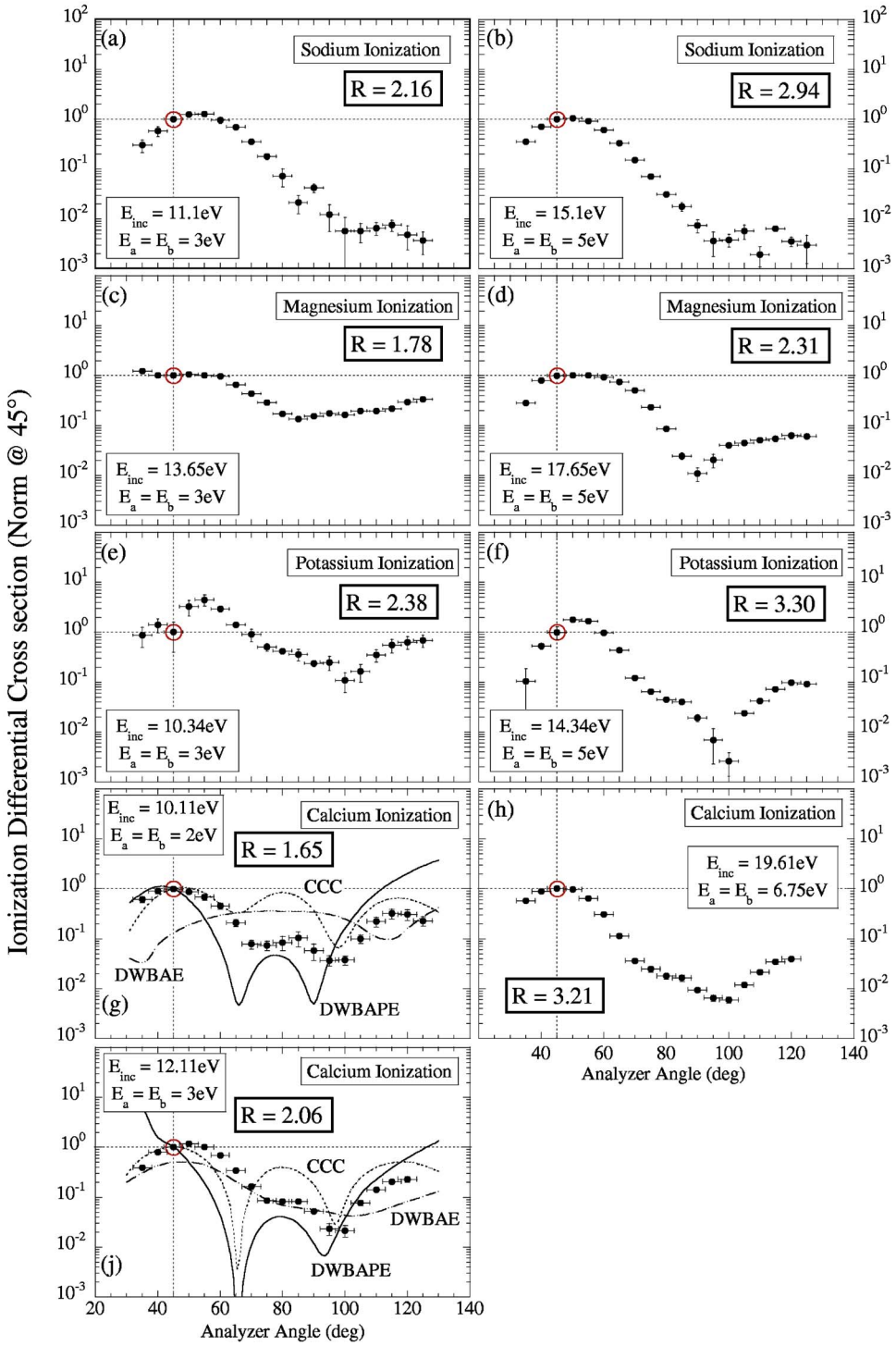

FIG. 5. (Color online) Experimental results near threshold for Na, Mg, K, and Ca, normalized to unity at $\theta=45°$. The results for Na, Mg, and K were taken with $E_a=E_b=3$ eV and 5 eV, whereas the results for Ca were taken for $E_a=E_b=3$ eV and 6.75 eV. DWBAE and DWBAPE theoretical curves are from [23], whereas the CCC curves are from [24]. For details, see text.

dominance of PCI. The experimental data at these low energies confirm this explanation.

At the higher energies where $E_a=E_b=2.5$ eV and 5 eV, there is clear evidence that PCI is still affecting the ionization process, however some structure emerges in the forward and backward directions. This is clearest when $E_a=E_b=5$ eV, where two distinct peaks are seen in the forward and backward direction. The forward peak at $\theta\sim 55°$ is considered to result from a single binary collision between the incident electron and target electron, the equal masses of the electrons requiring a mutual scattering angle near 90°. Since the experiment only measures events from electrons at *equal* scattering angles, this peak is then seen near $\theta_a=\theta_b=45°$. In a similar way, the backward peak at $\theta\sim 125°$ is considered to result from elastic scattering into the backward direction of the incident electron from the core, followed by a binary collision with a bound electron. The cross section at 3 eV and 5 eV is larger in the backward direction compared to the forward direction, indicating the strength of this multiple scattering process at low energies. All normalized data above $\theta=45°$ are seen to be greater than unity for this target at these energies.

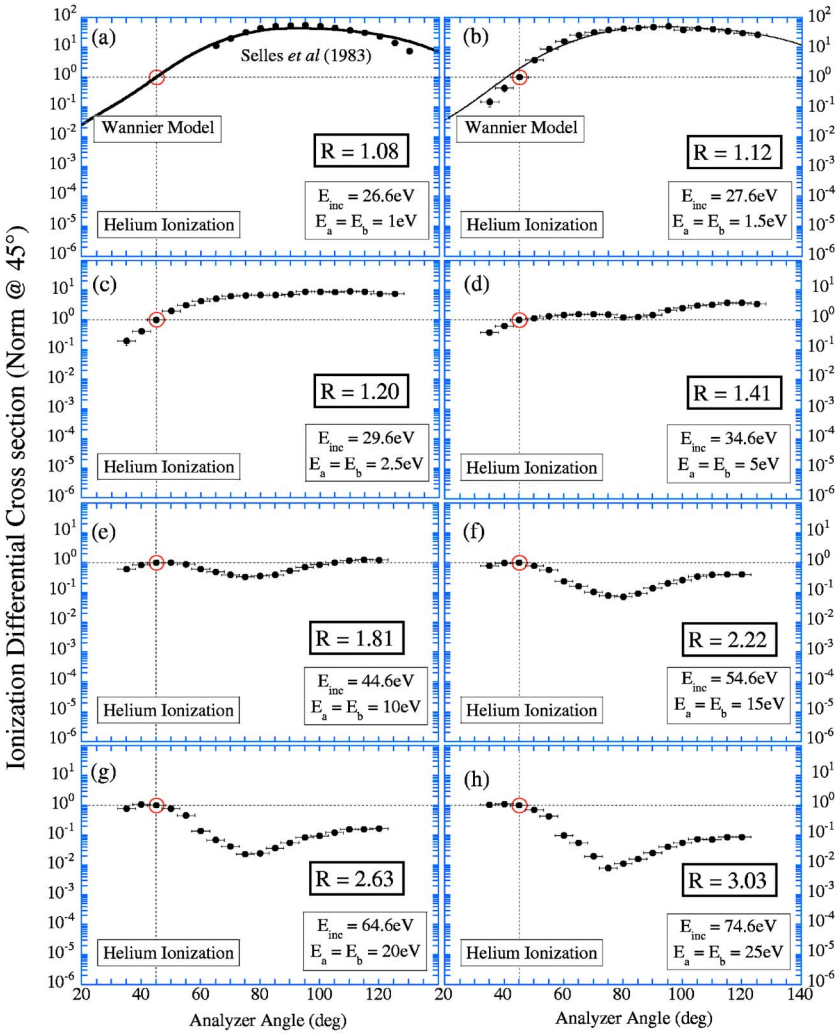

FIG. 6. (Color online) Results from helium over the same range of energies as in Figs. 7–10, normalized to unity at θ=45°. The cross section shows a smooth angular and peak height variation as the energy increases. Clear forward and backward structures are observed at higher energies, indicative of conventional binary and recoil scattering.

Discussion of results

Of interest in the data presented in Figs. 5 and 6 is the large difference between the results for helium and the metal vapor targets. PCI, which is essential when describing ionization of helium at low energies, is clearly not playing the same role for the more complex targets. Since PCI has importance *after the collision*, it is expected that this should affect electrons emerging from ionization of metal vapor targets in a similar way to those emerging from ionization of helium, redirecting electrons away from each other towards a scattering angle θ=90°.

The simple ideas discussed above which are considered reasonable for helium are clearly not applicable for the metal vapor targets, indicating that other more complex processes must be driving the reaction. Srivastava and co-workers [23] were the first to model the interaction for calcium, and include PCI using effective charges in the final state. They also include exchange in their calculation, which uses distorted waves in both incident and final channels. Their model indicates that at low energy [Figs. 5(g) and 5(j)], non-inclusion of PCI results in a broad, relatively featureless cross section (DWBAE). Once PCI is included (DWBAPE), peaks appear in their model at both forward and backward directions around θ=45° and 135°, as well as a third peak appearing around θ=80°. These features are qualitatively similar to experimental data, however the magnitudes do not agree. Interestingly, the CCC model of Bray and co-workers [24] (CCC) also produces a three-peak structure in the cross section at these energies, however their model does *not* include PCI.

A little surprising in the calculation of Srivastava and coworkers [23] is that the broad feature without PCI predicted at E_a=E_b=2 eV maximizes around θ=90°, and is roughly similar in shape to the results from the Wannier model in helium. Inclusion of PCI at this energy drastically alters this feature, resulting in three peaks, with dominance in the forward direction. It might be concluded from these results that the main peaks have evolved from electrons of equal energy travelling together in both the forward ($\theta \sim 0°$) and backward ($\theta \sim 180°$) directions, which is feasible if PCI is not included in the model. This process is obviously unphysical, the correct inclusion of the mutual Coulomb repulsion between the electrons driving them apart. It is not clear in such a model why the peak at θ=90° also appears once PCI is included. Unfortunately, the calculations of [23] do not include the results of the DWBAE model around 0° and 180°, so it is not possible to definitively draw conclusions from this.

It therefore remains uncertain why such a large difference between the helium results and the different metal vapors

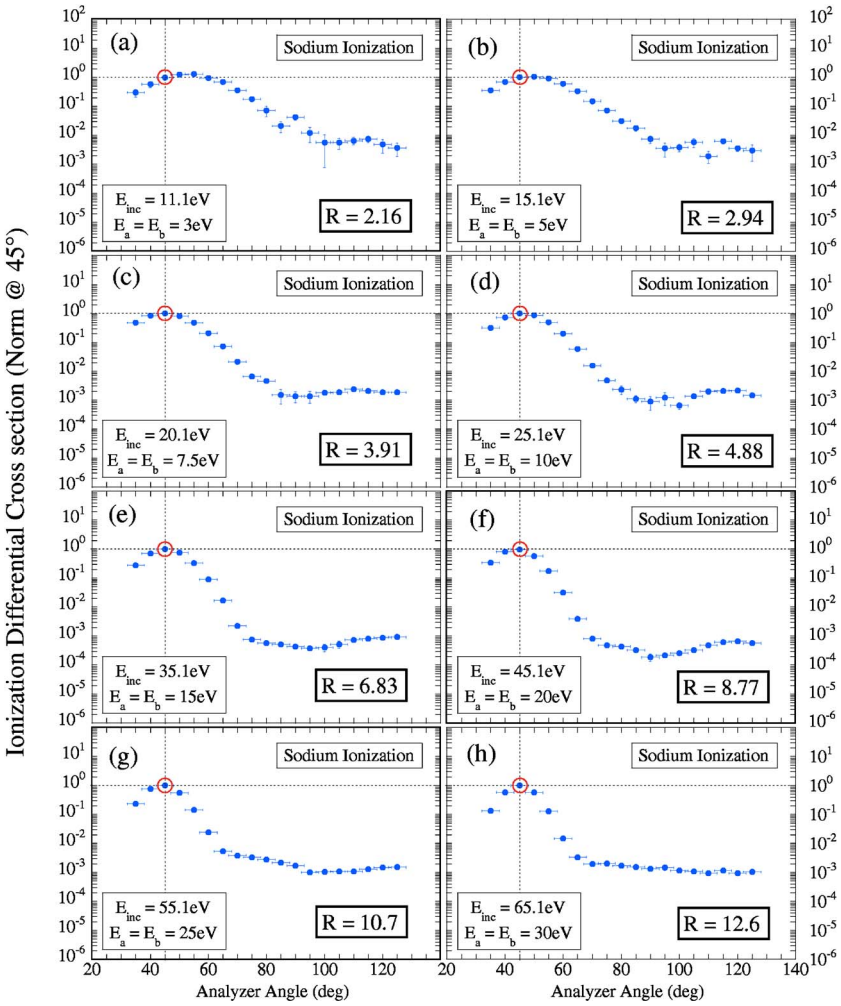

FIG. 7. (Color online) Full set of experimental results for Na, normalized to unity at θ=45°. The results show the evolution of the cross section with measured energy.

studied here is observed at these low energies. It is probable that the more complex electronic structure of the alkali-metal and alkali-earth-metal atoms is influencing the reaction, and that models which include interactions between the incident electron and the ensemble of target electrons will ultimately prove more accurate.

It should also be noted that direct comparison between theories which assume *mono-energetic* operating conditions, and actual experiments which have a finite energy resolution, must be carefully considered. As seen in Fig. 4, the coincidence energy resolution of the spectrometer has a finite half width of 560 meV, and so both *equal* and *nonequal* energy sharing reactions are measured *simultaneously* within this energy range. At high incident energies this energy balance is not expected to be significant, however at low energies where the cross section may change rapidly with both incident energy *and* energy sharing, it is likely that these effects will need to be resolved, before accurate comparison between theory and experiment can be made.

VII. INTERMEDIATE ENERGY RESULTS

The full set of experimental data for Na, Mg, K, and Ca are presented in Figs. 7–10, to allow a comprehensive comparison to be made between all results. By studying ionization from these targets, it should be possible to determine the effects of correlations between the valence electrons $(3s,3s^2)$ for (Na, Mg), $(4s,4s^2)$ for (K, Ca); together with any effects which occur due to the open $3d$ shell in K and Ca. Since each target has an increasingly complex electronic structure, it is also expected that this must be considered in any successful model of the collision. By obtaining data over a wide range of energies ranging from near threshold to around fifteen times the ionization potential, models which are successful in different energy regimes can be rigorously tested. It is hoped that this comprehensive set of data will aid significantly in the unification of all scattering models into a common theory for the ionization of atoms.

A. Sodium

Figure 7 shows the complete set of experimental data obtained from ionization of sodium. This target has been studied previously only in the high energy regime using either Electron momentum spectroscopy [36] or when ionization from a laser excited target was studied [37]. No other data is available at the low energies employed here.

The results are once again presented on a logarithmic scale, since there is a large variation in the cross section as the energy is varied. The results are for excess energies of (a)

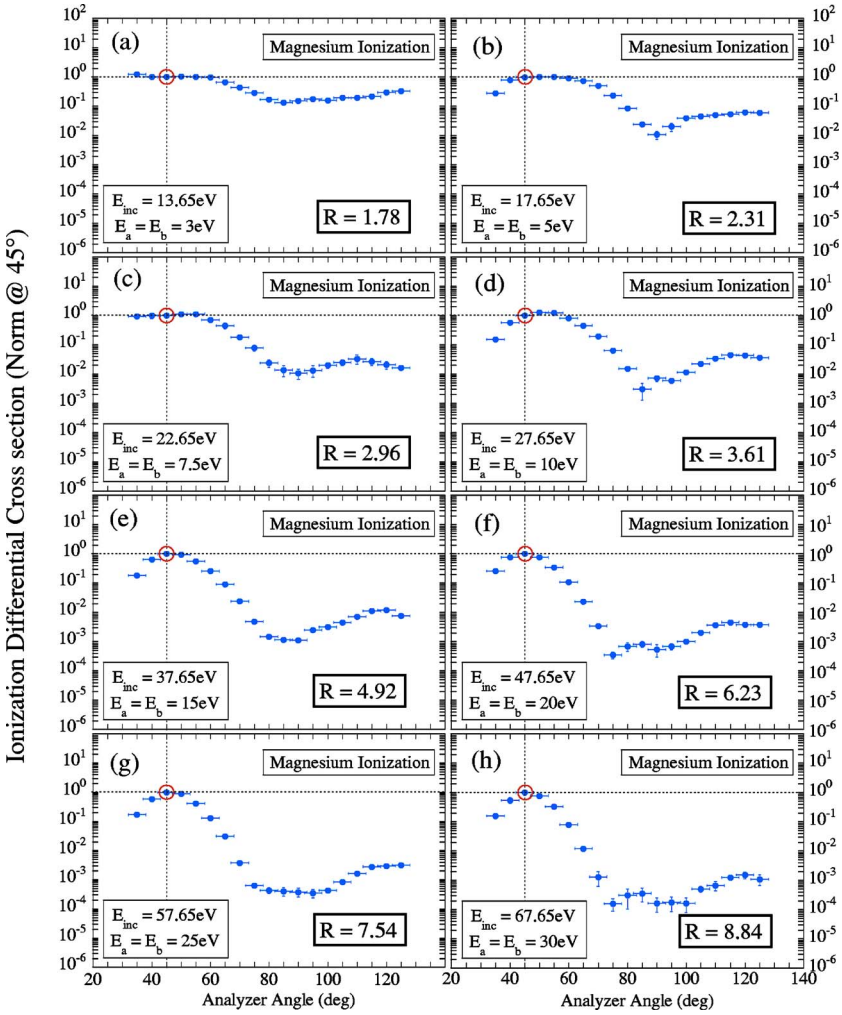

FIG. 8. (Color online) Full set of experimental results for Mg normalized to unity at θ=45°. The results show the evolution of the cross section with measured energy.

6 eV, (b) 10 eV, (c) 15 eV, (d) 20 eV, (e) 30 eV, (f) 40 eV, (g) 50 eV, and (h) 60 eV above the ionization threshold. All results are normalized to unity at θ=45°.

Inclusion of the complete data set for sodium in Fig. 7 allows the evolution of the cross section with energy to be seen. As noted in Sec. VI, the DCS at low energies shows a broad peaked structure which extends to $\theta \sim 100°$, before becoming relatively flat at higher angles. This forward scattering peak evolves into a narrower structure as the energy increases, the minimum progressively moving to lower angles. The backward scattering cross section remains relatively structureless and flattens out as the energy increases, until at $E_a=E_b=30$ eV the minimum is found at $\theta \sim 65°$ and the backward scattering cross section is uniform with angle. The relative cross section of this backward scattering feature is seen to steadily decrease, until at $E_a=E_b=20$ eV this reaches a minimum. At higher energies the relative magnitude of the backward structure increases with respect to the normalization point.

It is noted that these observations are *relative* measurements with respect to normalization at θ=45°. No attempt was made to place the results on an absolute scale due to the significant difficulties with the experiment. It was found necessary to vary the oven temperature and the incident electron beam current over a wide range when collecting these data, due to the very small cross sections observed at higher energies and due to the presence of uncorrelated scattered electrons at low energies. The variation in electron beam current produces a change in the size of the electron beam in the interaction region due to space charge, the change being both current and energy dependent. The change in oven temperature meant that it was not possible to evaluate a relative beam density in the interaction region. It should be possible to attempt renormalization of these data as a function of energy in the future, by adopting new techniques to determine the incident electron beam profile and atomic beam profile. These experiments to facilitate this are currently being considered, but are expected to be extremely difficult.

B. Magnesium

Figure 8 shows experimental results for magnesium, taken over the same outgoing electron energy range as for sodium. Unlike sodium which has a *single* 3*s* electron in the valence shell, magnesium has *two* 3*s* electrons, and the $3s^2$ shell is therefore closed. Assuming (to first order) that the inner electrons remain unaffected during the collision, the ionization cross section from magnesium might therefore be expected to be similar to that from helium, which has a $1s^2$ closed shell. Comparison with the helium results taken over the

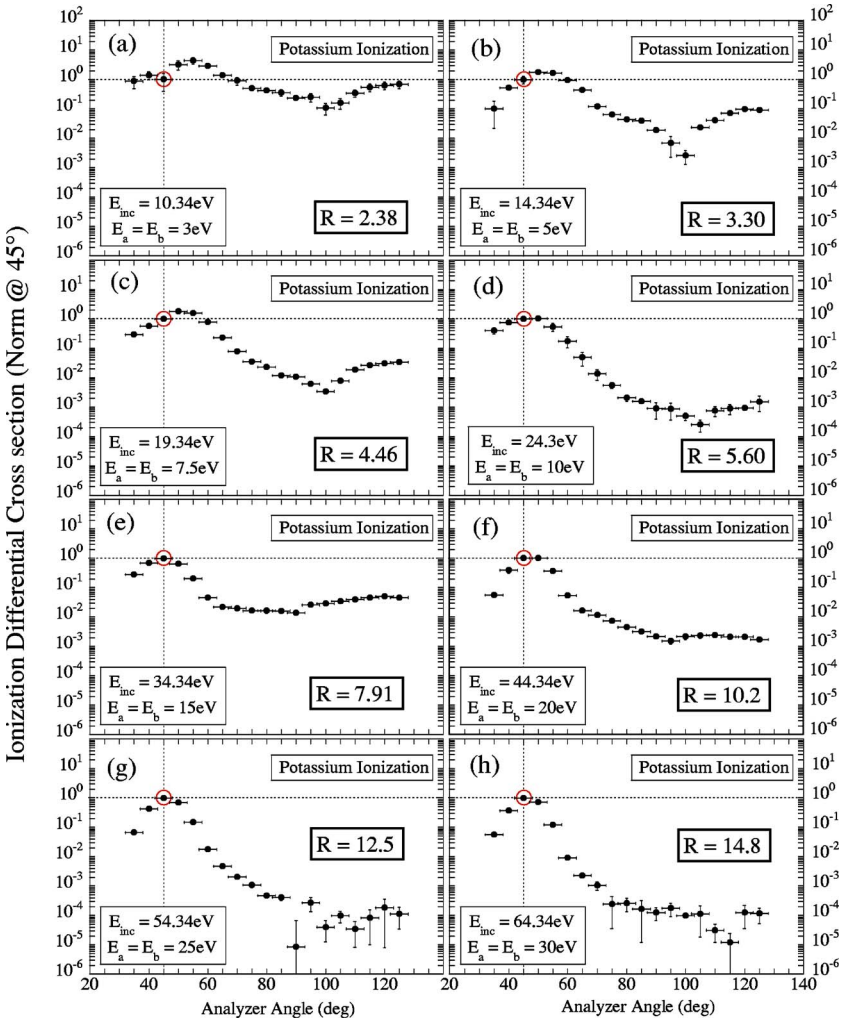

FIG. 9. (Color online) Full set of experimental results for K normalized to unity at θ=45°. The results show the evolution of the cross section with measured energy.

same energy range which are reproduced in Fig. 6 show that this expectation is broadly confirmed. As with helium, the cross section from magnesium displays a two peak structure, with the forward peak dominating over the backscatter peak at these energies. The minimum in the cross section occurs at $\theta \sim 80° - 85°$, again in common with data from helium, and the angle of the minimum changes little as a function of energy. At the lowest energy ($E_a = E_b = 3$ eV), the forward and backward peaks in Mg are of similar magnitude. The ratio between forward and backward peaks is seen to decrease monotonically with increasing energy. These variations are also observed in helium (Fig. 6), occurring at different outgoing electron energies but at similar values of R.

The results for magnesium do not show the same tendency to "flatten out" as observed in the other alkali-metal and alkali-earth-metal targets studied here. As with sodium, the variation in cross section over the accessed energy range is large, the DCS at $E_a = E_b = 30$ eV for magnesium showing a variation in excess of 6000:1. This contrasts with the results for helium in Fig. 6, which show a maximum variation of ~125:1 at $E_a = E_b = 25$ eV. This difference in the ratio of cross sections may be due to the much higher value of R=8.8 for magnesium, compared to R=3.0 for helium at these respective energies.

C. Potassium

Ionization differential cross section measurements from potassium are shown in Fig. 9, again using the same excess energy as for magnesium and sodium. Potassium has a single electron in the 4 s valence shell, which is preferentially filled prior to the 3d shell (filling of the 3d shell gives rise to the first series of transition elements in the Periodic Table). As such, it is likely that ionization from both potassium and calcium will be influenced by this open 3d shell, in contrast to both sodium and magnesium where all shells are filled sequentially.

The results for potassium show a clear difference to data from both magnesium and sodium, as might be expected from the more complex configuration of this target. At low energies, the forward peak has a magnitude greater than unity, since the maximum occurs at $\theta \sim 55°$ for this target. This peak position is similar to that in sodium, except that the peak in potassium is narrower. A new feature appears as a "shelf" type structure around $\theta \sim 80°$ in potassium. This occurs at a similar position to the more clearly defined middle peak in calcium at low energies, as discussed in Sec. VI. The minimum in the cross section occurs at $\theta \sim 100°$ as found for sodium. Unlike sodium however, a clear backward

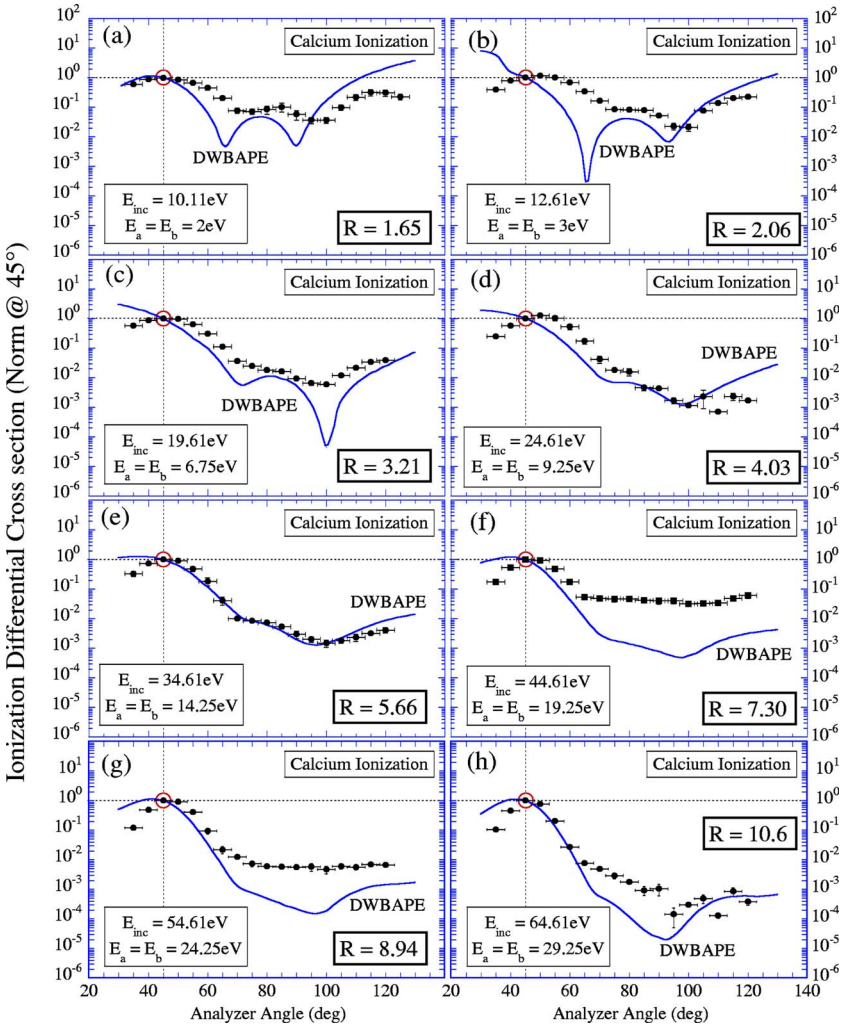

FIG. 10. (Color online) Full set of experimental results for Ca normalized to unity at θ=45°. The results show the evolution of the cross section with measured energy. The DWBAPE theory of [23], renormalized to unity at θ=45°, is also shown for comparison.

peak is evident at lower energies, which continues to be visible until E_a=E_b=10 eV.

At excess energies greater than 30 eV (E_a=E_b=15 eV), the results for potassium look similar to those for sodium at 50 eV excess energy [Fig. 7(g)], and to results for calcium at ~40 eV excess energy [Fig. 10(f)]. In common to all these results is a general "flattening" of the cross section at higher angles, together with an increase in the relative cross section which then steadily decreases as the energy increases. As an example, at E_a=E_b=10 eV in potassium, the ratio between maximum and minimum in the cross section is ~3800:1. By contrast, when E_a=E_b=15 eV this ratio has decreased to ~75:1, whereas at 60 eV excess energy the ratio has risen to ~50 000:1. It is this very large variation in the measured cross sections that requires the results for these targets to be placed on a relative scale spanning eight orders of magnitude.

The experimental data at higher energies show significant variation at larger angles due to the very low coincidence count rates obtained. This is reflected in the large error bars representing one standard deviation. Although the variation is large, it is still possible to establish the general trend, and to note that little variation in the cross section is seen as a function of angle.

D. Calcium

Experimental results for the ionization of calcium are reproduced in Fig. 10. These have been published previously [22] and are reproduced here for completeness, together with the theoretical results of [23] renormalized to unity at θ=45°. The data were taken at a slightly different set of energies than for the other targets, although the range that is covered is very similar. Of note is that it was possible to measure data for E_a=E_b=2 eV, which is lower than for all other targets, apart from helium. The low energy results have been discussed in detail in Sec. VI, and it is possible to see from Fig. 10 how the ionization cross section evolves with energy. From this complete set of results, it is seen that the middle peak at θ~80° remains visible when E_a=E_b=6.75 eV, although the feature is small. From discussions of the helium data shown in Fig. 6, it seems unlikely that this feature arises solely from PCI, which is not expected to play a significant role in producing a maximum near θ=90° for outgoing electrons of energy more than a few electron volts above threshold. The middle feature is not observed when E_a=E_b=9.25 eV, yet reappears when E_a=E_b=14.25 eV. It is possible that the feature is masked by the poorer statistics at the lower energy.

At an energy where $E_a=E_b=19.25$ eV, there is a marked change in the observed cross section compared to results at lower energies. As discussed for potassium, the ratio of maxima to minima markedly differs, being $\sim 720:1$ when $E_a=E_b=14.25$ eV compared to $\sim 25:1$ when $E_a=E_b=19.25$ eV. Again as for potassium, the structureless feature at higher scattering angles gradually decreases in magnitude as the energy increases, until at $E_a=E_b=29.25$ eV the ratio is $\sim 7500:1$. The uncertainty in the data at this energy is once again due to the very low count rates obtained from experiment.

E. Comparison between results

The data presented in Figs. 7–10 indicates that the ionization cross section varies in a complex way depending on the energy, scattering angle and type of target which is ionized. Similarities between the alkali-metal targets have been noted in the discussions above, as are contrasts between alkali-earth-metal targets. Similarities are also found for targets whose valence electrons reside in a shell with the same principle quantum number. A distinct feature only present in calcium and potassium is the middle structure occurring around $\theta \sim 80°$, and it may be that this is a signature of the open $3d$ shell for these targets. The featureless "shelf" in the cross section at higher energies first observed in calcium [22] has also now been seen in potassium and in sodium, but does not appear in magnesium at the energies adopted here. To observe this feature in three different targets at quite different energies indicates that this is not an experimental artefact, and must be explained.

For completeness and comparison, experimental results for ionization of helium are reproduced in Fig. 6, over an energy range from $E_a=E_b=1$ eV [34] through to $E_a=E_b=25$ eV [17,35]. Helium is the lightest target that can easily be studied, has only two electrons which reside in the $1s^2$ valence shell and so has no inner structure apart from the nucleus, which can be considered as a point charge. The results in Fig. 6 show that PCI dominates the interaction up to around 5 eV excess energy where the Wannier model can no longer be considered accurate, and that at higher energies the cross section evolves into two distinct peaks in the forward and backward direction. The ratio between the forward and backward scattering peaks smoothly and monotonically increases as the energy increases, the position of the minimum changing little over the range of energies adopted. The cross section for helium in a coplanar symmetric geometry has been modelled reasonably successfully by a number of different theories, including DWBA and CCC calculations. As such, confidence can be assigned to the description of the physical processes detailing different observed features, as have been discussed above.

When studies from the metal vapor targets commenced, it was thought that the results for the alkali-earth-metal atoms would be similar to helium, and that results for alkali-metal targets would show effects due to correlation between valence electrons. While similarities are certainly found with the helium results (in particular for magnesium), the data also shows that the interaction is far more complex for these multielectron targets. Different theories [23,24] recently applied to the data for calcium show marked discrepancies between theories and with experiment. The new results presented here show that these discrepancies are significant, other targets producing the same unusual variation in cross sections with energy as found for calcium. These differences must be explained before any model can be considered successful. The experimental data presented here spans an energy range from near threshold to beyond the intermediate energy regime, and so provides the most complete set of data currently available. It remains to be seen whether any single theory can be developed to satisfactorily explain the results over all energies.

VIII. CONCLUSIONS

Experimental results have been presented for alkali-metal and alkali-earth-metal targets from near threshold through to fifteen times the ionization potential. The data were taken in a coplanar symmetric geometry with the outgoing electrons sharing the excess energy from the reaction equally. The results for calcium are compared to new theoretical calculations, and the complete set of data has been contrasted to previous results from ionization of helium.

The objectives of this work were to provide a detailed set of accurate experimental data from ionization of complex targets over a wide energy range. It is felt that these objectives have been satisfied. The experimental techniques which were adopted have been detailed, as have the significant difficulties found with these targets. The results, collected over a three year period, will provide a challenge for current theories of the ionization process. It is hoped that the results will drive theory to develop new models which can be applied over a wide range of energies for many different targets.

Although the data presented here are comprehensive, they are by no means complete. Ideally the results should be placed on an absolute scale, so that rigorous comparison to future theory can be made. Placing the data on an absolute scale is a significant challenge in any low energy scattering experiment. For the metal vapor targets and low electron beam energies used here, this will be extremely difficult, since the atomic beam and electron beam profiles in the interaction region must be accurately known. It should be possible to ascertain the atomic beam density profile using laser-based fluorescence techniques, since laser excitation is possible for all targets studied here (provided the appropriate continuous wave lasers are available). It should also be possible to determine the electron beam characteristics within the interaction region, however this must be achieved while the oven is operating, to allow for variations in the electron spectrometer as detailed in Sec. II. Both methods are currently being considered, and may be implemented in future experiments at Manchester.

ACKNOWLEDGMENTS

The Engineering and Physical Sciences Research Council, UK is thanked for providing funding which allowed the

(e,2e) spectrometer to be modified for these studies. Alan Venables and Dave Coleman are gratefully acknowledged for providing continual technical support for the apparatus. The mechanical and electrical workshops in the Schuster Laboratory at Manchester are thanked for building the oven and power supplies.

[1] I. E. McCarthy and E. Weigold, Rep. Prog. Phys. **54**, 789 (1991).
[2] T. Rosel, J. Roder, L. Frost, K. Jung, H. Ehrhardt, S. Jones, and D. H. Madison, Phys. Rev. A **46**, 2539 (1992).
[3] G. Stefani, L. Avaldi, and R. Camilloni, J. Phys. IV **3**, 1 (1993).
[4] B. Rouvellou, S. Rioual, A. Pochat, R. J. Tweed, J. Langlois, Vein G. Nguyen, and O. Robaux, J. Phys. B **33**, L599 (2000).
[5] A. Lahmam-Bennani, J. Electron Spectrosc. Relat. Phenom. **123**, 365 (2002).
[6] C. C. Jia, A. Lahmam-Bennani, A. Duguet, L. Avaldi, M. Lecas, and C. Da Cappello, J. Phys. B **35**, 1103 (2002).
[7] J. Ullrich, R. Moshammer, A. Dorn, R. Dorner, L. P. H. Schmidt, and H. Schmidt-Bocking, Rep. Prog. Phys. **66**, 1463 (2003).
[8] B. A. deHarak, C. Zangjin, D. H. Madison, and N. L. S. Martin, J. Phys. B **38**, L145 (2005).
[9] M. Stevenson, G. J. Leighton, A. Crowe, K. Bartschat, O. K. Vorov, and D. H. Madison, J. Phys. B **38**, 433 (2005).
[10] F. W. Byron and C. J. Joachain, Phys. Rep. **179**, 211 (1989).
[11] X. Zhang, C. T. Whelan, and H. R. J. Walters, J. Phys. B **23**, L509 (1990).
[12] S. Rioual, A. Pochat, F. Gelebart, R. J. Allan, C. T. Whelan, and H. R. J. Walters, J. Phys. B **28**, 5317 (1995).
[13] R. H. G. Reid, K. Bartschat, and A. Raeker, J. Phys. B **31**, 563 (1998).
[14] J. Berakdar, H. Klar, M. Brauner, and J. S. Briggs, Z. Phys. D: At., Mol. Clusters **16**, 91 (1990).
[15] B. H. Bransden and C. J. Joachain, *Physics of Atoms and Molecules*, 2nd ed. (Prentice Hall, Harlow, 2003).
[16] A. J. Murray, B. C. H. Turton, and F. H. Read, Rev. Sci. Instrum. **63**, 3346 (1992).
[17] A. J. Murray and F. H. Read, Phys. Rev. A **47**, 3724 (1993).
[18] A. J. Murray and F. H. Read, Phys. Rev. Lett. **69**, 2912 (1992).
[19] A. J. Murray, M. B. J. Woolf, and F. H. Read, J. Phys. B **25**, 3021 (1992).
[20] A. J. Murray and F. H. Read, Phys. Rev. A **63**, 012714 (2000).
[21] N. J. Bowring, A. J. Murray, and F. H. Read, J. Phys. B **32**, L57 (1999).
[22] A. J. Murray and D. Cvejanovic, J. Phys. B **36**, 4875 (2003).
[23] R. K. Chauhan, M. K. Srivastava, and R. Srivastava, Phys. Rev. A **71**, 032708 (2005).
[24] I. Bray (private communication).
[25] G. H. Wannier, Phys. Rev. **90**, 817 (1953).
[26] J. A. Nelder and R. A. Mead, Comput. J. **7**, 308 (1965).
[27] "Photonis imaging sensors," www.photonis.com.
[28] A. J. Murray, Meas. Sci. Technol. **13**, N12 (2002).
[29] A. J. Murray and S. Atkinson, Meas. Sci. Technol. **15**, N31 (2004).
[30] D. Cvejanovic and A. J. Murray, Meas. Sci. Technol. **13**, 1482 (2002).
[31] Heater type 2ZE I 10/30-100/TI/CB 10/KZ 05 06/1.5m; www.Thermocoax.com.
[32] Thermocouple:2AB I 10/300mm/TI/MF9/2AB 25T.NN/2m; www.Thermocoax.com.
[33] J. N. H. Brunt, G. C. King, and F. H. Read, J. Phys. B **10**, 1289 (1977).
[34] P. Selles, A. Huetz, and J. Mazeau, J. Phys. B **20**, 5195 (1987).
[35] N. J. Bowring, A. J. Murray, and F. H. Read, J. Phys. B **30**, L671 (1997).
[36] E. Weigold, Aust. J. Phys. **44**, 277 (1991).
[37] J. Lower, E. Weigold, J. Berakdar, and S. Mazevet, Phys. Rev. Lett. **86**, 624 (2001).